ELSEVIER

Journal of Physics and Chemistry of Solids 61 (2000) 315–320

JOURNAL OF PHYSICS AND CHEMISTRY OF SOLIDS

www.elsevier.nl/locate/jpcs

Application of a new virtual crystal approach for the study of disordered perovskites

N.J. Ramer[a,b,*], A.M. Rappe[a,b]

[a]*Department of Chemistry, University of Pennsylvania, Philadelphia, PA 19104-6323, USA*
[b]*Laboratory for Research on the Structure of Matter, University of Pennsylvania, Philadelphia, PA 19104-6323, USA*

Received 23 February 1999; accepted 26 May 1999

Abstract

The "virtual crystal" (VC) approach is a tractable way of studying configurationally disordered systems; the potentials which represent atoms of two or more elements are averaged into a composite atomic potential. This approach has the advantage that a single configuration with a smaller unit cell represents the disordered system. However, due to the different local environment of the virtual atom, some properties may not be reproduced. In this work, we develop a new virtual crystal approach and apply it to the study of the stress-induced phase transition in $Pb(Zr_{1/2}Ti_{1/2})O_3$. We compare four averaging algorithms for the construction of the virtual atom pseudo-potentials and we assess the accuracy of each by comparing with a superlattice prediction of the equations of state.

Keywords: A. Ceramics; A. Oxides; C. Ab initio calculations; D. Ferroelectricity; D. Phase transitions

1. Introduction

Perfectly periodic systems are often difficult to achieve experimentally. Moreover, nonuniform aperiodic systems often provide the greatest utility in many applications. In order for theory to reach the goal of modeling these systems, new methods must be employed that will incorporate inhomogeneities without necessitating the use of extremely large unit cells which would make the problem computationally intractable. One frequently used approach is to formulate a hybrid atom or virtual atom that takes into account all the inhomogeneities. While this virtual crystal approximation (VCA) [1] is incapable of differentiating local environmental features of real materials, it can be useful in ascertaining averaged properties.

Standard approaches for implementing the VCA within density functional theory involve real-space averaging of the component potentials into a virtual crystal (VC) potential. The use of the VCA in condensed matter physics has primarily focused on the study of semi-conducting solid solutions and ferromagnetic alloys. The VCA has been used very successfully throughout these fields for studying the dependence of structural and electronic properties on composition [2–5]. Many properties computed with the VCA were found to be in general agreement with experimental results. However, some VC calculations in the literature have shown large discrepancies from experiment and superlattice calculations [6,7]. The researchers attributed the breakdown of the VCA to the inability of the VCA to capture differences in ionicity and chemical bonding.

The goal of this paper is to examine the effectiveness of VCA to model ferroelectric solid solutions. Recent experimental evidence [8] suggests that doped ferroelectric materials are good candidates for modeling using the VCA. The goal of this paper is to examine the effectiveness of VCA to model ferroelectric solid solutions. This paper reports the first density functional calculations involving ferroelectric materials using the VCA. Because of the significant problems with current implementations of VCA, we have developed new methods for more accurately portraying the electronic behavior of a VC atom. Instead of simply averaging component pseudo-potentials after construction, we incorporate the averaging within the pseudo-potential construction. We show that these methods, which insure the proper electronic properties at the atomic level, also

* Corresponding author. Fax: +1-215-573-2112.
E-mail address: ramer@seuss.chem.upenn.edu (N.J. Ramer)

0022-3697/00/$ - see front matter
PII: S0022-3697(99)00300-5

Table 1
Construction parameters for the Ti, Zr and VC designed nonlocal pseudo-potentials (the Ti and Zr potentials were generated with the methods described in Refs. [10,13]; the VC potentials were generated using the methods described in text; core radii (r_c) are in atomic units, q_c are in $Ry^{1/2}$, step widths are in atomic units and step heights are in Ry)

Atom	Reference configuration	r_c	q_c	Step range	Step height
Ti	$3s^2 3p^6 3d^0$	1.32, 1.20, 1.40	7.07, 7.07, 7.07	0.00–1.15	5.49
Zr	$4s^2 4p^6 4d^0$	1.51, 1.51, 1.90	7.07, 7.07, 7.07	0.00–1.51	0.77
VC2	$s^2 p^6 d^0$			0.00–1.15	3.13
				1.15–1.51	0.39
VC3	$s^2 p^6 d^0$			0.00–0.83	8.17
				0.83–0.32	5.59
VC4	$s^2 p^6 d^0$	1.38, 1.51, 1.40	7.07, 7.07, 7.07	0.00–0.56	1.18
				0.56–0.79	1.34

provide the most accurate structural results. Future applications of the presented VC methods to other disordered systems are planned, including metal alloys, semi-conducting and magnetoresistive materials.

The paper is organized as follows. In Section 2, we describe four methods for constructing the VC atoms (two standard approaches and two new construction procedures). We present and discuss the results of solid-state calculations using the four VC atoms to determine structural and energetic properties of $Pb(Zr_{1/2}Ti_{1/2})O_3$ (PZT) under uniaxial stress in Section 3. We conclude the paper in Section 4.

2. Methodology

Before discussing our implementations of the VCA, we describe the generation of an atomic pseudo-potential. First, an electronic reference state is chosen, and an all-electron calculation is performed. From this calculation we obtain the all-electron potential ($\hat{V}_{AE}$), the total energy (E_{tot}^{AE}), the all-electron wave functions ($\phi_{nl}^{AE}(\vec{r})$) and their eigenvalues (ϵ_{nl}^{AE}). Then a pseudo-potential, $\hat{V}_{PS}$, and pseudo-wave functions are chosen to satisfy

$$(\hat{T} + \hat{V}_H[\rho] + \hat{V}_{XC}[\rho] + \hat{V}_{PS})|\phi_{nl}^{PS}\rangle = \epsilon_{nl}^{AE}|\phi_{nl}^{PS}\rangle \quad (1)$$

where $\hat{T}$ is the single-particle kinetic energy operator and $\hat{V}_H[\rho]$ and $\hat{V}_{XC}[\rho]$ are the self-consistent Hartree and exchange-correlation energy operators, respectively. The latter two operators are explicit functionals of the total charge density, $\rho(\vec{r})$, where $\rho(\vec{r}) = \sum_{nl} f_{nl}|\phi_{nl}^{PS}(\vec{r})|^2$. We require

1. $\hat{V}_{PS}(\vec{r}) = \hat{V}_{AE}(\vec{r})$ for $r \geq r_c$
2. $\phi_{nl}^{PS}(\vec{r}) = \phi_{nl}^{AE}(\vec{r})$ for $r \geq r_c$

where r_c is the core radius.

Typically, $\hat{V}_{PS}$ may be expressed as a sum of a local potential and l-dependent correction terms:

$$\hat{V}_{PS} = \hat{V}^{loc} + \sum_l \Delta\hat{V}_l \quad (2)$$

where $\hat{V}^{loc}$ is a local operator, diagonal in the real-space basis. For a fully separable nonlocal pseudo-potential [9], $\Delta\hat{V}_l$ is formed according to

$$\Delta\hat{V}_l^{NL} \equiv \frac{\Delta\hat{V}_l^{SL}|\phi_{nl}^{PS}\rangle\langle\phi_{nl}^{PS}|\Delta\hat{V}_l^{SL}}{\langle\phi_{nl}^{PS}|\Delta\hat{V}_l^{SL}|\phi_{nl}^{PS}\rangle} \quad (3)$$

where $\Delta\hat{V}_l^{SL}$ are short-ranged correction terms to the local potential. We have recently formulated a new method for improving the transferability of nonlocal pseudo-potentials by altering the form of the local potential and subsequently the correction terms. A detailed discussion of the designed nonlocal (DNL) pseudo-potential method has been presented elsewhere [10]. We have used this approach in both new VC procedures.

Since our pseudo-potentials will ultimately be used in plane-wave basis solid-state calculations, we require the computation of $V(\vec{q},\vec{q}')$ where $\vec{q}$ and $\vec{q}'$ are reciprocal-space vectors. Using the notation from above, a local potential can be expressed as

$$\hat{V}^{loc} = \sum_{\vec{q}}\sum_{\vec{q}'}|\vec{q}'\rangle V^{loc}(|\vec{q}-\vec{q}'|)\langle\vec{q}| \quad (4)$$

Similarly, the nonlocal correction terms may be expressed as

$$\Delta\hat{V}_l^{NL} \equiv \sum_{\vec{q}}\sum_{\vec{q}'}\frac{|\vec{q}'\rangle\langle\vec{q}'|\Delta\hat{V}_l^{SL}|\phi_{nl}^{PS}\rangle\langle\phi_{nl}^{PS}|\Delta\hat{V}_l^{SL}|\vec{q}\rangle\langle\vec{q}|}{\langle\phi_{nl}^{PS}|\Delta\hat{V}_l^{SL}|\phi_{nl}^{PS}\rangle} \quad (5)$$

Based on these forms, the local and nonlocal Fourier-space matrix elements may be tabulated as $\langle\vec{q}'|\hat{V}^{loc}|\vec{q}\rangle$ and $\langle\vec{q}'|\Delta\hat{V}_l^{SL}|\phi_{nl}^{PS}\rangle$. In addition, the denominator of Eq. (5), $\langle\phi_{nl}^{PS}|\Delta\hat{V}_l^{SL}|\phi_{nl}^{PS}\rangle$ must be stored.

The VC construction methods are described for the combination of two atoms (A and B) according to $A_\alpha B_\beta$ where $\alpha + \beta = 1$. In addition, we restrict our description to homovalent atoms. These methods can be easily generalized to the averaging of more than two atoms and heterovalency. A more detailed explanation of these methods and their atomic and solid-state testing will be presented elsewhere [11].

Table 2
Configuration testing for the Ti, Zr and VC atoms generated with Methods 2–4 described in text (averaged eigenvalues are given for the Ti and Zr all-electron (AE) and component pseudo-potentials (PS); absolute errors are computed as a difference from the averaged component pseudo-potential results; all energies are in Ry)

State	AE $\frac{1}{2}$(Ti + Zr) energy	PS $\frac{1}{2}$(Ti + Zr) energy	VC2 error	VC3 error	VC4 error
s^2	−7.5701	−7.5701	0.2108	0.0000	0.0000
p^6	−5.9530	−5.9530	0.1554	0.0000	0.0000
s^0	−2.5554	−2.5581	0.0437	0.0003	−0.0038
d^0	−3.4488	−3.4488	0.2607	0.0000	0.0000
s^2	−6.7832	−6.7808	0.1942	−0.0017	0.0016
p^6	−5.1737	−5.1720	0.1398	−0.0005	0.0015
s^1	−2.0292	−2.0304	0.0335	−0.0020	−0.0009
d^0	−2.7037	−2.7034	0.2362	0.0044	0.0041
s^2	−6.3611	−6.3652	0.1434	0.0128	−0.0031
p^6	−4.7701	−4.7744	0.0923	0.0143	−0.0049
s^0	−1.8390	−1.8399	0.0147	0.0020	0.0000
d^1	−2.3479	−2.3571	0.1782	0.0163	−0.0033
s^2	−5.6569	−5.6586	0.1266	0.0100	−0.0029
p^6	−4.0711	−4.0734	0.0764	0.0123	−0.0047
s^1	−1.3449	−1.3453	0.0119	0.0004	0.0011
d^1	−1.6814	−1.6889	0.1549	0.0169	−0.0018
s^2	−4.1762	−4.1730	0.0398	0.0053	−0.0077
p^6	−2.6089	−2.6064	−0.0059	0.0086	−0.0106
s^2	−0.3301	−0.3293	−0.0097	−0.0002	0.0018
d^2	−0.3205	−0.3239	0.0586	0.0129	−0.0072

2.1. VC Method 1: Fourier averaging

This method relies on the Fourier-space representation of the pseudo-potentials as described above. Once the component potentials are expressed numerically as shown above, the matrix elements of the pseudo-potentials for atoms A and B are averaged.

2.2. VC Method 2: simple descreened pseudo-potential averaging

In this method, the descreened pseudo-potentials ($\hat{V}_{\mathrm{PS}}$) for the component pseudo-atoms are averaged. Two independent component atomic pseudo-potentials ($\hat{V}^{\mathrm{A}}_{\mathrm{PS}}$ and $\hat{V}^{\mathrm{B}}_{\mathrm{PS}}$) are constructed. These potentials are then averaged according to

$$\hat{V}^{\mathrm{VC2}}_{\mathrm{PS}} = \alpha\hat{V}^{\mathrm{A}}_{\mathrm{PS}} + \beta\hat{V}^{\mathrm{B}}_{\mathrm{PS}} \tag{6}$$

The semilocal potential alone is not sufficient for constructing a Kleinman–Bylander nonlocal pseudo-potential; the semilocal pseudo-wavefunctions must also be known (see Eq. (3)). Therefore, we solve for the reference-state pseudo-wavefunctions of $\hat{V}^{\mathrm{VC2}}_{\mathrm{PS}}$ and use these to construct the nonlocal potential.

2.3. VC Method 3: tuned descreened pseudo-potential averaging

The previous two constructions do not guarantee accurate representation of the electronic properties of a true hybrid atom. In order to improve the electronic behavior of the VC potential, we impose a new criterion in our VC construction. We introduce an averaged eigenvalue

$$\epsilon^{\mathrm{AVG}}_{nl} = \alpha\epsilon^{\mathrm{A}}_{nl} + \beta\epsilon^{\mathrm{B}}_{nl} \tag{7}$$

where $\epsilon^{\mathrm{A}}_{nl}$ and $\epsilon^{\mathrm{B}}_{nl}$ are the all-electron eigenvalues for the nlth state of atoms A and B, respectively. We construct a VC potential which guarantees that $\epsilon^{\mathrm{VC3}}_{nl} = \epsilon^{\mathrm{AVG}}_{nl}$ for the reference state by adjusting the parameters used to average the semilocal potentials. This may be expressed as

$$\hat{V}^{\mathrm{VC3}}_{\mathrm{PS}} = \alpha'\hat{V}^{\mathrm{A}}_{\mathrm{PS}} + \beta'\hat{V}^{\mathrm{B}}_{\mathrm{PS}} \tag{8}$$

where α' and β', in general, will not equal α and β. Subsequently, we repeat the process described in Method 2 to obtain the necessary pseudo-wavefunctions and construct a nonlocal potential. We then construct a DNL potential to improve eigenvalue agreement at other electronic configurations.

2.4. VC Method 4: all-electron potential averaging

In all the previous constructions, we average together two pseudo-potentials at various points in their construction. In this method, we average all-electron results, thereby enforcing reference-state eigenvalue agreement throughout the entire pseudo-potential construction. First, the bare nuclear

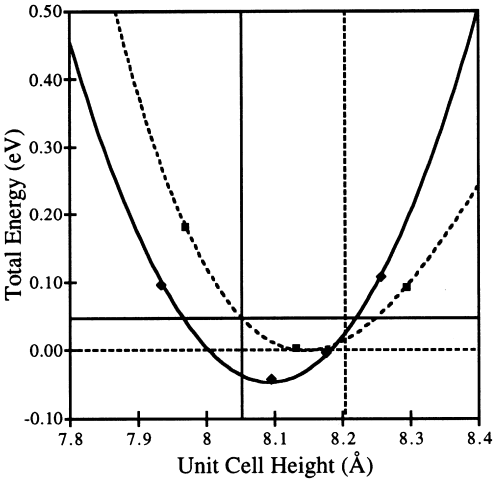

Fig. 1. Equations of state for the tetragonal (dotted-line) and rhombohedral-like (solid-line) phases of $Pb(Zr_{1/2}Ti_{1/2})O_3$ using VC Method 1 as described in text. The intersection of the solid straight lines indicates the position of the superlattice equilibrium cell height and ground-state energy for the rhombohedral-like phase. The intersection of the dotted straight lines shows the placement of the tetragonal phase ground-state structure. The heights and energies are for a 40-atom unit cell.

Coulombic potentials of the component atoms are averaged:

$$V_{\mathrm{AE}}^{\mathrm{VC4}}(\vec{r}) = \alpha V_{\mathrm{AE}}^{\mathrm{A}}(\vec{r}) + \beta V_{\mathrm{AE}}^{\mathrm{B}}(\vec{r}) = \frac{-2(\alpha Z_{\mathrm{AE}}^{\mathrm{A}} + \beta Z_{\mathrm{AE}}^{\mathrm{B}})}{r} \quad (9)$$

In addition, we determine a core charge density that is the average of the core charge densities of the all-electron component atoms,

$$\rho_{\mathrm{core}}^{\mathrm{VC4}} = \alpha \rho_{\mathrm{core}}^{\mathrm{A}} + \beta \rho_{\mathrm{core}}^{\mathrm{B}} \quad (10)$$

Using this nuclear potential and frozen-core charge density, we find new all-electron wavefunctions for valence states. We accomplish this by completing a self-consistent inward solve [12] for the valence wavefunctions according to

1. $\epsilon_{nl}^{\mathrm{AVG}} = \epsilon_{nl}^{\mathrm{VC4}}$
2. $\phi_{nl}^{\mathrm{VC4}}(r) \rightarrow 0$ as $r \rightarrow \infty$
3. $\int_{r_c}^{\infty} |\phi_{nl}^{\mathrm{VC4}}(r)|^2 r^2 \, \mathrm{d}r = \alpha \int_{r_c}^{\infty} |\phi_{nl}^{\mathrm{A}}(r)|^2 r^2 \, \mathrm{d}r + \beta \int_{r_c}^{\infty} |\phi_{nl}^{\mathrm{B}}(r)|^2 r^2 \, \mathrm{d}r$

Operationally, we complete an inward solve well below r_c, insuring accurate first and second derivative determination for all values of r greater than r_c. These derivatives are required for the optimized pseudo-potential construction.

Since the form of these all-electron VC wavefunctions will be modified within the core region when the wavefunctions are pseudized [13], the Kohn–Sham equations need not be solved between $r = 0$ and $r = r_c$. We construct the remainder of the wavefunction as a smooth analytic form insuring norm-conservation and agreement with the inward solution. A new valence charge density is constructed, and the process is iterated to self-consistency. These wavefunctions are self-consistent solutions to the Kohn–Sham equation outside r_c, with eigenvalues and total norm outside r_c which are exactly the average of the component atoms. With this set of wavefunctions and eigenvalues we construct a single optimized semilocal pseudo-potential. From this potential, a DNL pseudo-potential is then constructed.

3. Results and discussion

We have applied the four averaging methods to the Ti and Zr atoms. All atomic energy calculations were done within the local density approximation, and the optimized pseudo-potential [13] and DNL [10] methods were used. The generation parameters for these component potentials and the VC potentials are included in Table 1. For all atoms, semi-core states were included as valence. It is important to note that although we have included multiple *s*-channel states, only one nonlocal projector is included. For all atoms we have used the *s*-potential as the local potential onto which we add one or two square-step augmentation operators. The transferability data for the VC atoms generated with Methods 2–4 are presented in Table 2. For completeness, we have included the transferability data for the DNL component pseudo-potentials as well as the all-electron averaged eigenvalues. (We do not include the transferability data for Method 1 since the Fourier averaging procedure makes real-space atomic testing inconvenient.) All errors are computed as the difference from the averaged DNL pseudo-potential results. From the table, it is clear that Method 4 provides the most transferable potentials.

In order to test the accuracy of these potentials in solid-state calculations, we have completed first-principles calculations using density functional theory (DFT) and the local density approximation. The electron wavefunctions are expanded in a plane-wave basis using a cutoff energy of 50 Ry. In addition to the semi-core states mentioned above, the 5d shell is included in the Pb potential. Scalar relativistic effects are included in the generation of the Pb pseudo-potential [14]. Brillouin zone integrations are approximated accurately as sums on a $4 \times 4 \times 4$ Monkhorst–Pack *k*-point mesh [15].

We have applied uniaxial stress along the (100) direction to two structurally distinct phases of PZT. For each of the four VC methods, we have completed full electronic and structural relaxations for 5-atom unit cells with various fixed cell heights. We have neglected the shear response to the uniaxial stress in the present study.

Experimentally, the equilibrium structure for the 50/50 composition of PZT is a tetragonal phase down to low temperature [16]. The rhombohedral phase has been found to lie close in energy to the tetragonal phase, and phase transition to the rhombohedral structure can be induced when uniaxial stress is applied to this material [17–20].

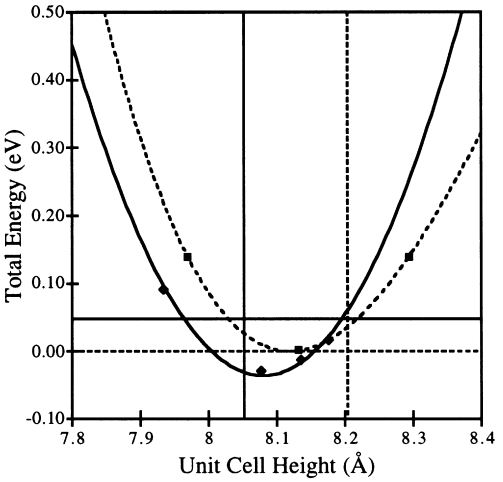

Fig. 2. Equations of state for the tetragonal (dotted-line) and rhombohedral-like (solid-line) phases of $Pb(Zr_{1/2}Ti_{1/2})O_3$ using VC Method 2 as described in text.

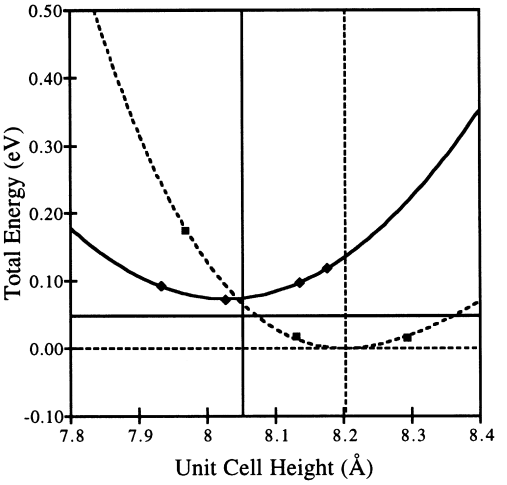

Fig. 4. Equations of state for the tetragonal (dotted-line) and rhombohedral-like (solid-line) phases of $Pb(Zr_{1/2}Ti_{1/2})O_3$ using VC Method 4 as described in text.

An experimental lattice constant of 8.163 Å has been determined for the rhombohedral phase of a randomly ordered ceramic with 50/50 batch composition [21]. A lattice constant of 8.279 Å for the tetragonal phase has also been reported.

Using a superlattice DFT approach, we have recently computed the phase stability and critical stress for 50/50 PZT [22]. These theoretical results agree well with experimental findings; for the current work, the superlattice equations of state provide a benchmark by which to judge the accuracy of the VCA calculations. For each VC method, we have plotted the equations of state (total energy as a function of unit cell height) for the two phases of PZT in Fig. 1–4.

The intersection of the solid straight lines in each plot represents the ground-state energy and equilibrium lattice constant for a 40-atom rhombohedral structure of a superlattice of PZT. The dotted straight lines show the analogous values for the tetragonal phase of the same superlattice. For clarity, Fig. 5 contains the equations of state for the superlattice of PZT. Details of these superlattice calculations have been presented elsewhere [22].

For VC Methods 1 and 2, we find that the ground-state phase for this composite of PZT is rhombohedral, in direct opposition to the superlattice calculations and experimental observations. However, for Methods 3 and 4, we find the correct energetic ordering, with the tetragonal phase lower

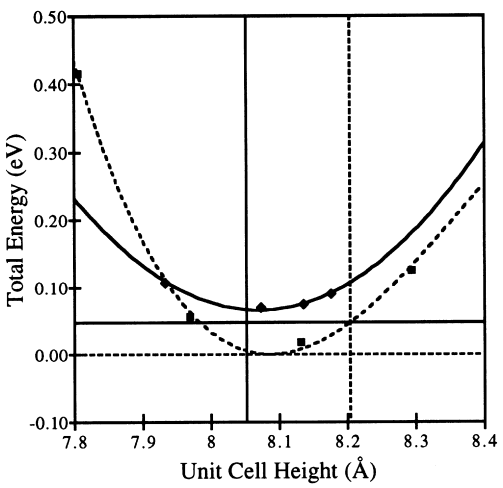

Fig. 3. Equations of state for the tetragonal (dotted-line) and rhombohedral-like (solid-line) phases of $Pb(Zr_{1/2}Ti_{1/2})O_3$ using VC Method 3 as described in text.

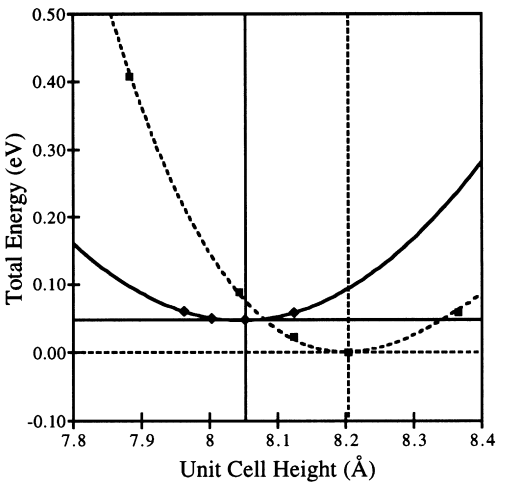

Fig. 5. Equations of state for the tetragonal (dotted-line) and rhombohedral-like (solid-line) phases of $Pb(Zr_{1/2}Ti_{1/2})O_3$ using a superlattice.

in energy than the rhombohedral. For Method 3, we find that the predicted equilibrium unit cell heights are nearly identical and therefore do not show two distinct metastable phases. For Method 4, we find well-separated equations of state, in excellent agreement with the superlattice results. These lattice parameters are also in good agreement with the experimental findings (~1% lower as expected with the local density approximation). From the equations of state we also determine the critical stress required to induce phase transition. This can be computed using a Gibb's construction. From our superlattice calculations, we have found that a stress of 669 MPa is necessary to cause the transition from the rhombohedral-like phase to the tetragonal phase. For VC Method 4, we compute a stress of 830 MPa for this same phase transition.

4. Conclusions

In this paper we have developed new methods for constructing VC pseudo-potentials and applied the VC approximation to the Ti and Zr atoms. We have described four methods for averaging the component atoms and have determined the electronic properties of a 1:1 ratio of these atoms. As a means for comparison, we have completed density functional calculations for two competing phases of $Pb(Zr_{1/2}Ti_{1/2})O_3$. Comparison of the results to those of superlattice calculations shows that methods which include accurate averaging of the electronic properties (Methods 3 and 4) yield the proper energetic ordering of the two phases. Method 4, in particular, provides excellent agreement with superlattice calculations and experimental results. We have shown the applicability of the VC approach to studying compositional disorder in perovskite solid solutions. This approach permits more complicated structures to be studied while maintaining computational tractability. Studies involving heterovalent atoms as well as ternary component potentials may provide even greater utility for these methods.

Acknowledgements

The authors would like to thank Ilya Grinberg for his help with the all-electron potential averaging virtual crystal method. This work was supported by NSF grant DMR 97-02514 and the Petroleum Research Fund of the American Chemical Society (Grant no. 32007-G5) as well as the Laboratory for Research on the Structure of Matter and the Research Foundation at the University of Pennsylvania. Computational support was provided by the San Diego Supercomputer Center and the National Center for Supercomputing Applications.

References

[1] L. Nørdheim, Ann. Phys. (Leipzig) 9 (1931) 607.
[2] S. de Gironcoli, P. Giannozzi, S. Baroni, Phys. Rev. Lett. 66 (1991) 2116.
[3] N. Marzari, S. de Gironcoli, S. Baroni, Phys. Rev. Lett. 72 (1994) 4001.
[4] D.A. Papaconstantopoulos, W.E. Pickett, Phys. Rev. B 57 (1998) 12 751.
[5] P. Slavenburg, Phys. Rev. B 55 (1997) 16 110.
[6] C. Chen, E.G. Wang, Y.M. Gu, D.M. Bylander, L. Kleinman, Phys. Rev. B 57 (1998) 3753.
[7] L. Bellaiche, S.-H. Wei, A. Zunger, Appl. Phys. Lett. 70 (1997) 3558.
[8] W. Windsch, M.K. Gergs, D. Michel, H. Schlemmbach, A. Salzer, P. Reich, Ferroelectrics 109 (1990) 119.
[9] L. Kleinman, D.M. Bylander, Phys. Rev. Lett. 48 (1982) 1425.
[10] N.J. Ramer, A.M. Rappe, Phys. Rev. B 59 (1999) 12471.
[11] N.J. Ramer, A.M. Rappe, Phys. Rev. B (1999) submitted.
[12] C. Froese, Can. J. Phys. 41 (1963) 1895.
[13] A.M. Rappe, K.M. Rabe, E. Kaxiras, J.D. Joannopoulos, Phys. Rev. B 41 (1990) 1227.
[14] D.D. Koelling, B.N. Harmon, J. Phys. C 10 (1977) 3107.
[15] H.J. Monkhorst, J.D. Pack, Phys. Rev. B 13 (1976) 5188.
[16] B. Jaffe, W.R. Cook Jr., H. Jaffe, Piezoelectric Ceramics, TechBooks, Marietta, OH, 1990.
[17] A.H. Meitzler, H.M. O'Bryan Jr., Appl. Phys. Lett. 19 (1971) 106.
[18] E.T. Keve, A.D. Annis, Ferroelectrics 5 (1973) 77.
[19] E.T. Keve, Appl. Phys. Lett. 26 (1975) 659.
[20] K. Kakegawa, J. Mohri, S. Shirasaki, K. Takahashi, J. Am. Ceram. Soc. 65 (1982) 515.
[21] B. Jaffe, R.S. Roth, S. Marzullo, J. Res. Nat. Bur. Stand. 55 (1955) 239.
[22] N.J. Ramer, S.P. Lewis, E.J. Mele, A.M. Rappe, in: R.E. Cohen (Ed.), First-Principles Calculations for Ferroelectrics—Fifth Williamsburg Workshop, AIP, Woodbury, NY, 1998, p. 156.